New hemispheric geomagnetic indices α with 15 min time resolution

Aude Chambodut, Aurélie Marchaudon, Chantal Lathuillère, Michel Menvielle, Etienne Foucault

AGU PUBLICATIONS

JGR

Journal of Geophysical Research: Space Physics

RESEARCH ARTICLE

10.1002/2015JA021479

Key Points:
- Calculation of new 15 min, hemispheric and planetary, subauroral geomagnetic indices
- Use of an adaptive network of stations along time
- New indices enhance subauroral magnetic activity description

Correspondence to:
A. Chambodut,
aude.chambodut@unistra.fr

Citation:
Chambodut, A., A. Marchaudon, C. Lathuillère, M. Menvielle, and E. Foucault (2015), New hemispheric geomagnetic indices α with 15 min time resolution, *J. Geophys. Res. Space Physics*, *120*, 9943–9958, doi:10.1002/2015JA021479.

Received 21 MAY 2015
Accepted 18 OCT 2015
Accepted article online 22 OCT 2015
Published online 14 NOV 2015

New hemispheric geomagnetic indices α with 15 min time resolution

Aude Chambodut[1], Aurélie Marchaudon[2,3], Chantal Lathuillère[4,5], Michel Menvielle[6,7], and Etienne Foucault[2,3]

[1]Institut de Physique du Globe de Strasbourg, UMR7516, Université de Strasbourg/EOST, CNRS, Strasbourg, France, [2]Université de Toulouse, UPS-OMP, IRAP, Toulouse, France, [3]CNRS, IRAP, Toulouse, France, [4]Université Grenoble Alpes, IPAG, Grenoble, France, [5]CNRS, IPAG, Grenoble, France, [6]Université de Versailles St-Quentin, LATMOS-IPSL, CNRS-INSU UMR 8190, Guyancourt, France, [7]Département des Sciences de la Terre, Université de Paris-Sud, Orsay, France

Abstract New subauroral α_{15} indices are proposed. They are based on a simple reproducible algorithm which relies on an as dense as possible network of magnetic observatories in each hemisphere. At first, the variation with time of local geomagnetic activity is determined at each magnetic station. Gathering all obtained stations' precomputed values, a normalization with corrected geomagnetic latitude is determined. Then, for each 15 min interval, magnetic activity on the horizontal component is averaged out over 15 min and corrected using this normalization, before a spline modeling of the longitudinal variation in each hemisphere is applied. Hemispheric and planetary 15 min indices are then computed by arithmetic means. Preliminary statistical results, from probability distribution function over a solar cycle and superposed epoch analysis during storms conditions, show, by comparison with *am* geomagnetic index series, that new α_{15} indices are reliable in describing subauroral magnetic activity. These new indices will suit any future user, allowing either to choose the spatial description (planetary versus hemispheric) and/or to choose the temporal resolution, knowing unambiguously all their strengths and caveats.

1. Introduction

Magnetic observatories record variations of magnetic activity at the Earth's surface since as early as 1840. *Lockwood* [2013] proposed very interesting historical reviews about geomagnetic activity observations and their connections with solar-terrestrial coupling. From the beginning of the twentieth century, geomagnetic indices were designed and routinely calculated in order to obtain integrated and pertinent information about the Earth's magnetic activity variations. The 3 h magnetic activity *K* index was proposed at the end of the 1930s by *Bartels et al.* [1939], and 3 h *K*-derived planetary magnetic indices using *K* indices from a network of observatories were introduced from the 1940s. On a planetary scale, three main indices were proposed: *Kp* [*Bartels*, 1949], *am*, and *aa* [*Mayaud*, 1968, 1973], the main difference between these three indices lying in the observatory network used in their derivation. Among these global indices, the *am* index is one of the most pertinent to characterize the Earth's magnetosphere-ionosphere activity and its coupling with the solar wind [*Svalgaard*, 1977], as it is based on magnetic stations quite evenly distributed in longitude at subauroral latitudes.

Other indices were also developed in parallel in order to follow magnetic activity associated with specific current systems in the magnetosphere: the *Dst* index [*Sugiura*, 1965] followed by the *SYM* index [*Iyemori*, 1990] dedicated to currents that produce axially symmetric magnetic disturbances, such as the ring current, the magnetopause current, and the magnetotail current; the *ASY* index [*Iyemori*, 1990] dedicated to longitudinally asymmetric disturbances; the *AE*, *AU*, and *AL* indices [*Davis and Sugiura*, 1966] designed to follow auroral electrojet activity; and finally, the *PC* index [*Troshichev et al.*, 1988] aimed at monitoring the magnitude of the transpolar convection electric field in each hemisphere and statistically following the solar wind merging electric field. A detailed description of all these indices can be found in *Menvielle et al.* [2011].

Such indices are extremely useful for describing magnetic activity and are almost systematically used as inputs for models: physical or semiempirical models describing a specific region of the Earth's environment (e.g., radiation belts, plasmasphere, thermosphere, or ionosphere). A large majority of these models use the *Kp* planetary index as input. Nevertheless, its 3h temporal resolution does not enable one to accurately

reproduce the global dynamics of the modeled system. Moreover, some of these models could benefit from more regional description of the activity.

Since a few years, sustained efforts have been made to propose new magnetic indices, allowing a better description of the magnetosphere-ionosphere system, its energy inputs due to its coupling with the solar wind and the interplanetary magnetic field (IMF), and the different system of currents arising from this coupling. Two major purposes are pursued for these new indices. First, for main and crustal fields modeling, the selection of quiet time magnetic satellite data would be greatly improved by a more accurate temporal and spatial description of geomagnetic disturbances, the external field spectrum overlapping partly with that of the internal field one [*Constable and Constable*, 2004; *Friis-Christensen et al.*, 2006]. Second, space weather development results in a need for new indices describing more precisely the Earth's electrodynamics as well as for identifying precisely the onset and the morphology of the events responsible for magnetosphere-ionosphere coupling enhancement (storms and substorms) for forecasting purposes.

For these new indices, several ways of improvement have been followed: a better spatial and/or temporal resolution, a different definition of the reference zero level in the magnetic variations [*Gjerloev*, 2012], and/or a completely different algorithmic for index calculation. It would be difficult to list exhaustively all the new proposed indices and their direct applications, but we can cite among them the following: the $a\lambda$ geographic longitudinal sector indices [*Menvielle and Paris*, 2001; *Thomson and Lesur*, 2007] proving good efficiency for selection of quiet time magnetic satellite data but not for description of the different sources of Earth's magnetic activity; the U.S. Geological Survey *Dst* [*Gannon and Love*, 2011; *Katus and Liemohn*, 2013] which, in comparison with the historical version of *Dst*, allows to better describe the response to magnetic storm events at low latitude and midlatitude regions; the *SME* family of indices [*Newell and Gjerloev*, 2011a, 2011b; *Singh et al.*, 2013] based on the same algorithmic as *AE* but with largely more stations to avoid missing some substorm commencement; the *SMR* indices [*Newell and Gjerloev*, 2012; *Haaland and Gjerloev*, 2013] allowing to describe the morphology of the ring current in different magnetic local time sectors with a large set of magnetic stations; the *Wp* index [*Nosé et al.*, 2012] allowing the identification of substorm onset through Pi2 wave activity. Finally, *Chambodut et al.* [2013] proposed the $a\sigma$ subauroral indices based on the *am* index derivation and covering four different magnetic local time (MLT) sectors: dawn (03–09 MLT), noon (09–15 MLT), dusk (15–21 MLT), and midnight (21–03 MLT) sectors. The major interest of these new indices lies in their retroactive calculation from 1959; however, they suffer the limitation inherent to their 3 h time resolution, preventing a good description of magnetospheric events, such as storms.

In this paper, we propose two new hemispheric subauroral indices, named α_{15N} and α_{15S}, based on a new algorithmic and on a new magnetometers network. The design of the α_{15} index is based on the same philosophy as the *am* index but with a higher temporal resolution. We thus chose the same initial letter of the alphabet: *a*. However, in order not to make any possible confusion with the International Association of Geomagnetism and Aeronomy (IAGA)-endorsed geomagnetic index *aa*, we chose to use the Greek alphabet letter, α, rather than the modern Latin alphabet one. The originality of these new indices lies in their temporal resolution of as low as 15 min. Planetary indices can be reconstructed by averaging indices of both hemispheres. We will call alpha family of indices, all the α indices derived from α_{15} but averaged over variable time intervals (e.g., α_{180} for α_{15} averaged over 180 min).

To avoid our new indices to be used as "a black box," they must be simple to calculate and easily reproducible. Moreover, to ensure operational constraints, related to, e.g., space weather nowcasting and forecasting, it is essential to circulate quicklook values of the indices in near real time. To answer these different requirements, the choice of both the algorithmic and the magnetometers network is crucial. The magnetic observatory data must be digital magnetometers, and the new algorithm must be designed so as to meet the needs for real-time index calculation (in particular, not to have to wait for the definitive data type produced yearly by magnetic observatories). Finally, the index calculation must be ensured despite the loss of one or several stations. Therefore, the index calculation will begin in 1996 when digital observatories started forming a reliable network using all the available stations in the subauroral latitude ranges.

The computation algorithm of these new α_{15} indices consists in four steps: (i) computation of the reference zero level every minute for each magnetic observatory; (ii) computation of the 15 min values of magnetic activity ΔH_{15} for each observatory; (iii) latitudinal correction for each observatory; and (iv) longitudinal fitting, once the observatory network is defined.

The first three steps are implemented on each observatory data separately and are presented in section 2. The data combination of the different stations, to compute the hemispheric indices onto the period 1996–2009, is described in section 3. Statistical analyses of the hemispheric and planetary indices behaviors are compared to *am* planetary index in section 4, over almost a solar cycle (i.e., 2000 to 2009) and during strong magnetic events. Section 5 presents the behavior of the α_{15} indices during two geomagnetic storm cases. Section 6 is dedicated to conclusion.

2. Characterization of the Geomagnetic Activity in Each Observatory

2.1. Analogies With *K* Index Calculation

For comparison with historical indices, we try to ensure the best possible consistency between our new indices and the long-lasting series of *K*-derived geomagnetic indices *aa* and *am*. This will impact on both the used time interval and reference zero level.

First, the experience gained with *K*-derived planetary geomagnetic indices shows that magnetic activity at subauroral latitudes can be characterized using magnetic variations measured in the two horizontal components; magnetic variations in the vertical component are not considered because they are more sensitive to internal induction effects [see, e.g., *Bartels et al.*, 1939; *Menvielle et al.*, 2011, and references therein]. We thus decided to base our new indices on the same magnetic components as the ones used for *K*-derived geomagnetic indices.

The magnetic signature of intense *Pc*5 geomagnetic pulsations (typically observed in the 150–600 s range) can correspond to oscillations with a significant amplitude at subauroral latitudes and is captured by minute values. The *K* index is a range index with a 3 h time resolution: it results in practice in a filtering out of such geomagnetic pulsations. Obviously, one of the aims of our new indices is to improve the temporal resolution, without capturing such *Pc*5 pulsations to ensure their consistency with the *aa* and *am* geomagnetic indices. In order to achieve a good *Pc*5 pulsation damping, we decided to have a 15 min time resolution for the new indices.

2.2. Definition of the Reference Zero Level

Since we aim at following geomagnetic variations at subauroral latitudes, we decided to use as a reference level the one used for *K* index derivation. This would enable us to take advantage of the experience acquired during decades of *K* index derivation.

The reference zero level that we use is defined as "a smooth curve to be expected for that element on a magnetically quiet day, according to the season, the sunspot cycle and, in some cases, the phase of the Moon" [*Bartels et al.*, 1939]. This reference level results in fact from two different contributions: the solar regular variation, S_R, that is mainly related to the atmospheric dynamo processes, and the slow recovery phase corresponding to the depression in the magnetic horizontal component due to the ring current at the end of and after a geomagnetic storm. The slow recovery phase is represented by the *Dst*.

We used the algorithm of the Finnish Meteorological Institute (FMI) [*Sucksdorff et al.*, 1991; *Menvielle et al.*, 1995] to determine the reference zero level. This reference zero level will be abusively named S_R variation in the following. It is determined independently for each of the two horizontal components through a regression over sliding windows of a size of 24 UT hours shifted on a daily basis.

In the original version of the FMI program, jumps in the S_R determination may appear between the S_R curves computed for two consecutive 24 h periods. Such jump has no impact on *K* determination since *K* is based on range in the magnetic variation, and the jump, if any, occurs at the limit between two consecutive 3 h intervals. On the contrary, such jump would impact the calculation of the 15 min index since its value directly depends on the S_R determination. The algorithm has therefore been adapted to allow a smooth continuous S_R variation curve along time. In practice, S_R curves are estimated using the FMI program over a sliding window of a size of 24 h shifted every UT hour. Figure 1 shows an example of reference zero level determination. We know from our experience of real-time *K* index determination that such a method can be used for an operational real-time quicklook value determination.

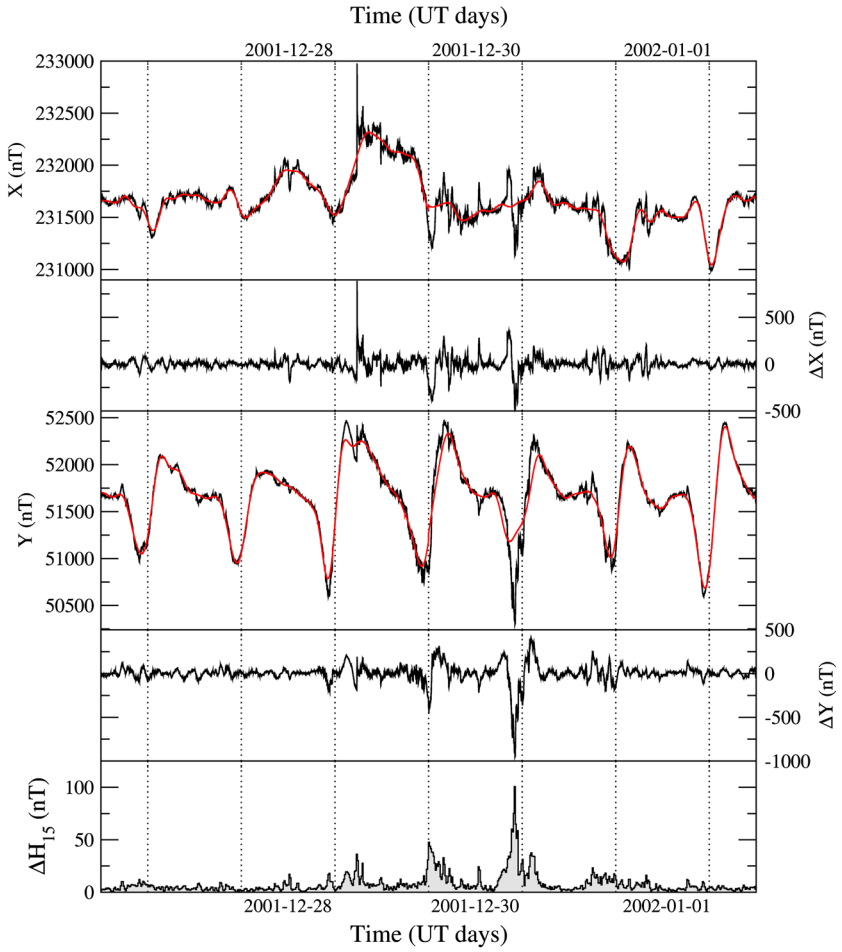

Figure 1. (top to bottom) X, ΔX, Y, ΔY, and ΔH_{15} variations for seven consecutive days, from noon 26 December 2001 to noon 2 January 2002, at the Canberra (CNB, Australia) magnetic observatory. The red curves superimposed on X and Y correspond to the S_R quiet curves calculated and removed to obtain ΔX and ΔY.

2.3. Fifteen-Minute ΔH Calculation in Each Observatory

After the calculation of the reference zero level curve, the magnetic variations in each horizontal components (X, Y) are obtained for each minute t:

$$\begin{cases} \Delta X(t) = X(t) - S_{R_X}(t), \\ \Delta Y(t) = Y(t) - S_{R_Y}(t). \end{cases}$$

The ΔX and ΔY values in nanotesla are then directly used for the determination of ΔH and its arithmetic mean over 15 min ΔH_{15}.

$$\Delta H(t) = \sqrt{(\Delta X(t))^2 + (\Delta Y(t))^2},$$

$$\Delta H_{15}(t) = \frac{1}{15} \sum_{i=1}^{15} \Delta H(t + i - 8).$$

We thus obtained the series of ΔH_{15} values for each magnetic observatory. Figure 1 shows the ΔX, ΔY, and ΔH_{15} variations for seven consecutive days (from 26 December 2001 to 2 January 2002) at the CNB (Canberra, Australia) magnetic observatory. One may see that 30 December is a magnetically disturbed day, while 27 and 28 December are quiet ones.

2.4. Latitudinal Correction

To characterize magnetic activity at subauroral latitudes, our new indices have to represent magnetic activity at ±50° corrected geomagnetic (CGM) latitude, as already proposed for historical indices by *Bartels* [1949]

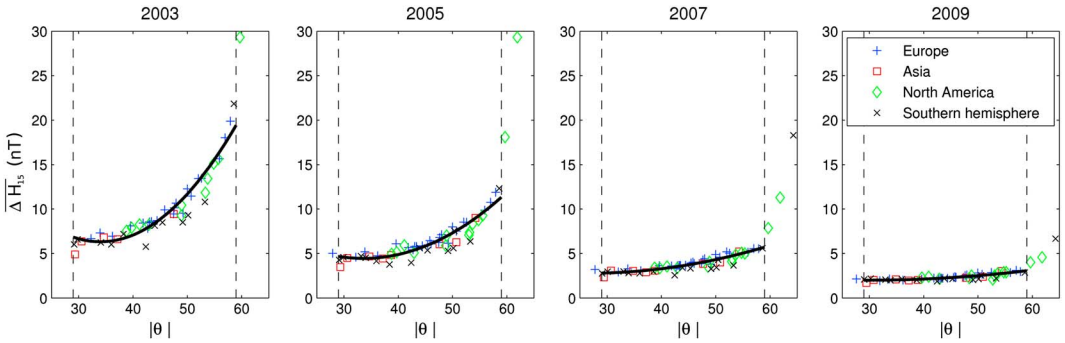

Figure 2. $\overline{\Delta H_{15}}$ values of INTERMAGNET observatories as a function of their yearly absolute CGM latitude $|\theta|$ for (left to right) 2003, 2005, 2007, and 2009. The solid line indicates the quadratic fit used to model the latitudinal variation of magnetic activity and calculated over the interval $|\theta| = [29°, 59°]$ (dashed vertical lines).

and *Mayaud* [1968]. This implies that we have to correct the ΔH_{15} observed in the different observatories for representing the activity at ±50° CGM latitude in the corresponding hemisphere.

Recall here that the CGM coordinates (first introduced by *Hakura* [1965]) of a point in space (latitude, longitude, and altitude) are computed by tracing the geomagnetic field line (i.e., calculated from Geomagnetic Reference Field DGRF/IGRF model) through the considered point to the dipole geomagnetic equator, then returning to the same altitude along the dipole field line, and, finally, assigning the obtained dipole (latitude and longitude) as the starting point CGM coordinates. Using CGM coordinates is thus more appropriate when considering magnetic variations that are related to ionospheric currents, the geometry of which is directly governed by that of the Earth's magnetic field. Note that using CGM coordinate system is in agreement with the conclusions of the recent paper of *Laundal and Gjerloev* [2014] who propose to use such a system for the *AL* and *SML* geomagnetic indices which monitor the westward ionospheric electrojet. From now on, CGM latitude will be denoted as θ ($|\theta|$ for its absolute value). CGM coordinates change with time, as a result of the secular variation of the Earth's geomagnetic field. This secular variation is therefore taken into account in the procedure used for the new index calculation by considering, for each magnetic station *S*, its CGM latitude θ computed at epoch *t* (1 July of related year): $\theta_S(t)$, described by the International Geomagnetic Reference Field (IGRF) model [*Thébault et al.*, 2015].

To study the general behavior of magnetic activity in subauroral zones, we present in Figure 2 examples of the latitudinal variations of the yearly mean values of ΔH_{15} (denoted $\overline{\Delta H_{15}}$ in the following) for several years and for all observatories with $25° \leq |\theta| \leq 65°$. On this figure, different symbols corresponding to different longitude sectors are used for the Northern Hemisphere observatories; only a single symbol is used in the Southern Hemisphere where observatories are not so many. The magnetic activity clearly follows a quadratic trend with respect to $|\theta|$, and the amplitude of the $\overline{\Delta H_{15}}$ variation depends on the solar cycle with a maximum in 2003 and a minimum in 2009, for which it almost vanished. It is worth noting that, for a given year, the latitudinal variation does not depend on the longitude sector. This would not have been the case if we had calculated the mean over periods smaller than the year, because of the UT seasonal variations of magnetic activity [see, e.g., *La Sayette and Berthelier*, 1996; *Cliver et al.*, 2000].

In the following, we restricted CGM latitudes $|\theta|$ to the range 29° and 59°. For each year between 1996 and 2008 (2009 being not used because of solar cycle 23 minimum specificity), we have fitted the observed variation of $\overline{\Delta H_{15}}$ with $|\theta|$ using quadratic functions $f(\theta, t)$, shown as solid curves in Figure 2:

$$f(\theta, t) = a(t).(|\theta| - 50)^2 + b(t).(|\theta| - 50) + c(t).$$

The 13 $f(\theta)$ functions are afterward normalized such that $f(\pm 50°) = 1$. The coefficients of the 13 *f*-normalized functions are averaged to obtain a mean quadratic curve of coefficients $(\overline{a}, \overline{b}, \overline{c})$ which allow to obtain a correction function cor which depends on $|\theta|$:

$$\mathrm{cor}(\theta) = 1/\left(\overline{a}.(|\theta| - 50)^2 + \overline{b}.(|\theta| - 50) + \overline{c}\right) \quad \text{if: } |\theta| \in [32.6°, 59.0°],$$
$$\mathrm{cor}(\theta) = 1/0.61 \quad \text{if: } |\theta| \in [29°, 32.6°],$$

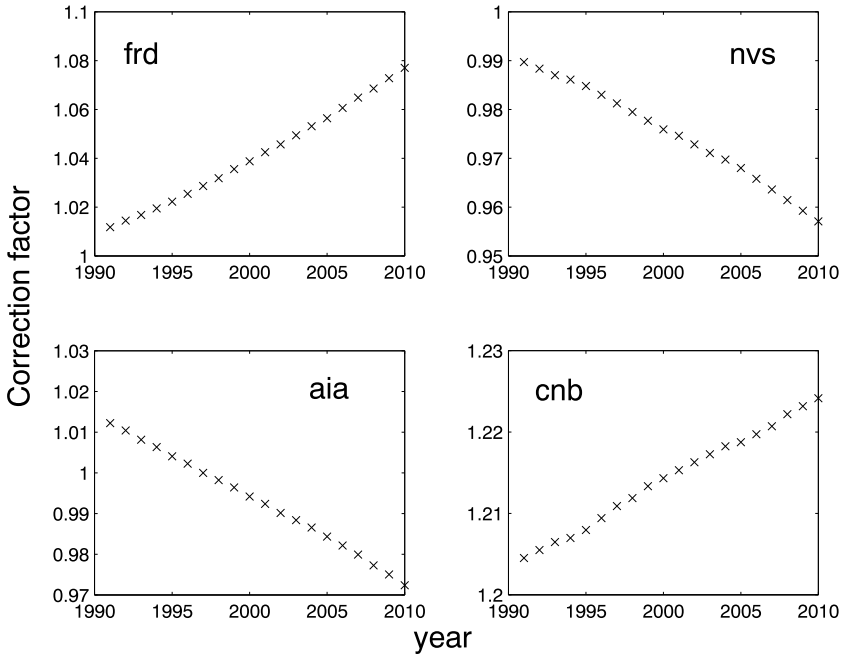

Figure 3. Correction factors cor as a function of time in years (1990–2010), for four observatories: FRD and NVS in the Northern Hemisphere and AIA and CNB in the Southern Hemisphere.

with $\overline{a} = 0.0013 \pm 0.0004$; $\overline{b} = 0.045 \pm 0.0050$; and $\overline{c} = 1 \pm 0.03$. The $(1/0.61)$ value for small $|\theta|$ aimed at having a monotonic cor(θ) function. In practice, it was only used in the Southern Hemisphere (see subsection 3.1 for details of network determination). The cor(θ) varies between 1.62 and 0.80 for $|\theta|$ increasing from 35° to 55° CGM latitude.

For each station S located at CGM latitude $\theta_S(t)$ on epoch t, a specific correction factor cor$(\theta_S(t))$ is deduced from this mean curve that may be seen as an abacus to rescale the magnetic activity at 50° CGM latitude; the corrected ΔH_{15} value is thus equal to $\left[\Delta H_{15}.\text{cor}(\theta_S(t))\right]$. As already stated, the cor$(\theta_S(t))$ coefficient takes into account the secular variation of the Earth's magnetic field through the variation with time of the CGM latitude of the station.

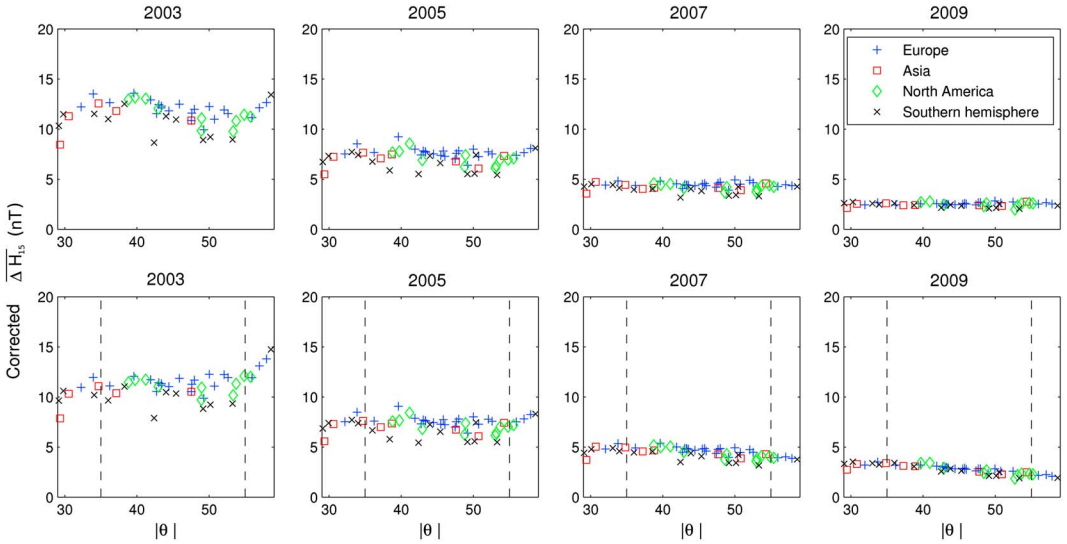

Figure 4. Corrected $\overline{\Delta H_{15}}$ values of all observatories as a function of their yearly absolute CGM latitude $|\theta|$. (top row) The used correction factor cor is deduced from the specific quadratic fit of $f(\theta, t)$ over the considered epoch t; and (bottom row) the used correction factor cor is deduced from the globally averaged correction function cor.

Table 1. List of Stations Used in the Derivation of α_{15} Indices With Respect to the Period

OBS	θ (CGM 2005)	ϕ (CGM 2005)	Period	OBS	θ (CGM 2005)	ϕ (CGM 2005)	Period
AAA	38.69	149.48	2005–2009	HAD	47.48	74.51	1996–2009
AIA	−50.35	9.17	2004–2009	HBK	−36.00	95.35	1999–2009
AMS	−49.18	138.99	1996–2009	HER	−42.40	82.94	1996–2009
AQU	36.23	87.28	2000–2009	HLP	50.74	94.97	1998–2009
ASP	−34.03	207.32	1999–2009	HRB	43.04	92.66	1997–2009
BDV	44.45	89.30	1996–2009	IRT	47.59	177.58	1999–2009
BEL	47.63	95.91	1996–2009	LRM	−33.16	185.82	2004–2009
BFE	52.07	89.25	1996–2008	LVV	45.47	98.07	2004–2009
BFO	43.58	84.25	2006–2009	MAB	46.05	82.57	2005–2009
BOU	48.91	320.11	1999–2009	MMB	37.16	215.77	1996–2009
BOX	54.25	113.12	2004–2009	NCK	42.75	91.31	1996–2009
BSL	41.14	340.91	1996–2005, 2007–2009	NEW	54.82	303.89	1996–2009
CLF	43.35	79.14	1996–2009	NGK	47.97	88.96	1996–2009
CNB	−45.40	226.98	1996–2009	NVS	50.72	156.11	2004–2009
CTA	−29.13	220.52	2000–2009	PST	−38.40	10.49	2003–2009
CZT	−53.28	106.25	1996–2009	SHU	53.03	259.07	2005–2009
DLR	38.79	326.72	1996–2007	STJ	53.15	31.27	1996–2009
DOU	45.84	81.62	2002–2009	SUA	39.61	99.39	2000–2009
ESK	52.59	77.02	1996–2009	THY	41.90	91.88	1996–2009
EYR	−50.16	256.54	1996–2009	TRW	−29.93	4.91	2000–2009
FRD	48.77	358.29	1996–2009	TUC	39.73	314.96	1996–2009
FRN	42.93	303.98	1996–2009	VAL	49.19	70.21	2002–2009
FUR	43.36	86.73	2000–2009	VIC	53.72	296.66	1996–2009
GNA	−43.98	187.31	1996–2009	WNG	50.00	86.45	1996, 1998–2009

Figure 3 shows some examples of the evolution of $\mathrm{cor}(\theta_S(t))$ as a function of time t at four stations: AIA (Argentine Islands, Antarctica) and CNB (Canberra, Australia) in the Southern Hemisphere, and FRD (Fredericksburg, United States) and NVS (Novosibirsk, Russian Federation) in the Northern Hemisphere. It illustrates the fact that the correction factors may vary a few percent in opposite directions over 20 years.

Figure 4 shows the effect of the latitudinal correction on the $\overline{\Delta H_{15}}$ values of each station for the years 2003 to 2009. In Figure 4 (top row), the used correction factor is deduced from the quadratic fit specific of the considered epoch t: $f(\theta, t)$, while in Figure 4 (bottom row) we used the averaged correction function $\mathrm{cor}(\theta)$. The comparison between the two rows of Figure 4 shows that using a single correction abacus for all years does not result in an increase of the data scatter. This supports the use of cor function for latitudinal correction. It may be, however, noticed that the cor function is not well adapted to very low geomagnetic activity periods as in 2009. Indeed, in that case, the corrected $\overline{\Delta H_{15}}$ values appear to be underestimated by about 0.5 to 1 nT at high latitude.

3. Fifteen-Minute α Index Calculation

3.1. Network

The network definition is the following element necessary to implement the α_{15} index calculation. In Figure 4, one can observe that variations with latitude do not disappear above $|\theta| = 55°$ latitude in 2003 and 2005, regardless of the correction used. Indeed, latitudes above $|\theta| = 55°$ may be inside the auroral oval when it expands toward the equator during magnetically active periods. Consequently, during periods of intense magnetic activity the observatories with CGM latitudes such as $|\theta| > 55°$ would not record subauroral magnetic activity and we excluded them from the network used for calculating our new indices. As the number of stations is large in the subauroral zone of the Northern Hemisphere, we decided to use 35° CGM latitude

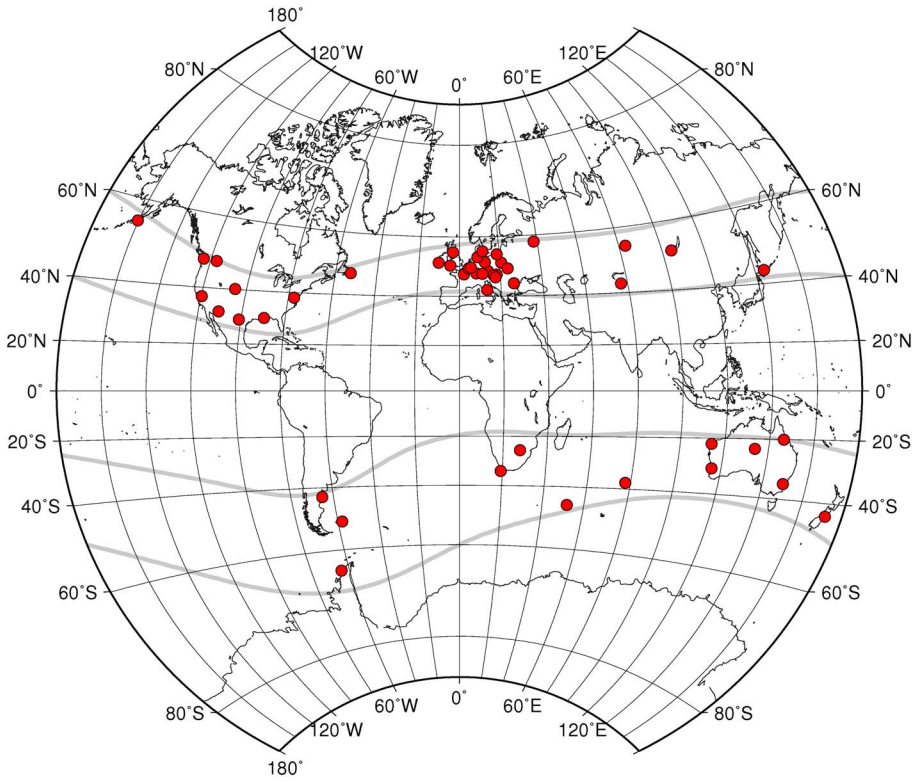

Figure 5. Geographic distribution of the 48 magnetic observatories of the α_{15} network. The light gray curves present the corrected magnetic longitudes 55°, 35°, −29°, and −55°, in 2000.

as a lower limit. In the Southern Hemisphere, we added the few stations situated between −29° and −35° in order to obtain a better distribution of the stations in longitude.

Therefore, the network used for our new α_{15} indices will be defined every year, so as to include for a given year all the stations of the INTERMAGNET network [*Kerridge*, 2001] located between 35° and 55° north and south absolute CGM latitudes, plus a few ones located between 29° and 35° in the Southern Hemisphere. Table 1 gives a list of these stations, with the indication of the years between 1996 and 2009 for which they have been used. Figure 5 shows the corresponding distribution of magnetic observatories (all years). The number of stations tends to increase with time from 20 stations in the Northern Hemisphere and 6 in the Southern Hemisphere for year 1996, to a maximum of, respectively, 35 and 13 stations for year 2007. Over the 14 year period, a mean of 38 stations (28 over the Northern Hemisphere and 10 over the Southern Hemisphere) have been used. It has to be noted that we chose to use only stations that provided INTERMAGNET magnetic data over more than four consecutive years over the period 1996–2009. KIV (Kiev, Ukraine) in the Northern Hemisphere and KMH (Keetmanshoop, Namibia) and TDC (Tristan Da Cunha, UK) in the Southern Hemisphere became part of the INTERMAGNET Network in 2009. Moreover, GCK (Grocka, Serbia) data were only available in 2005 and 2007–2009 and PAG (Panagjurishte, Bulgaria) data in 2007–2009. Consequently, the data of these five observatories have not been used here. They will, however, be included in future calculation of definitive values of the α_{15} indices.

3.2. Hemispheric Fitting in Longitude

The corrected ΔH_{15} values are a set of discrete points distributed over the whole longitude range in each hemisphere. In order to get for each 15 min interval a smooth representation of the variation with longitude of the magnetic activity at ±50° CGM latitude, a nonparametric adjustment by smoothing cubic splines of the corrected ΔH_{15} is applied independently for each hemisphere (labeled N and S) along CGM longitude ϕ. Two continuous scalar functions $\alpha_{15N}(\phi)$ and $\alpha_{15S}(\phi)$ are obtained. The spline fitting is performed according to an algorithm described by *Silverman* [1985]. It includes a cross-validation estimate of the balance between fitting and smoothing. A 95% pointwise probability confidence interval $\delta\alpha$, based upon a Bayesian approach, is also derived using the B-spline expression of the set of cubic splines.

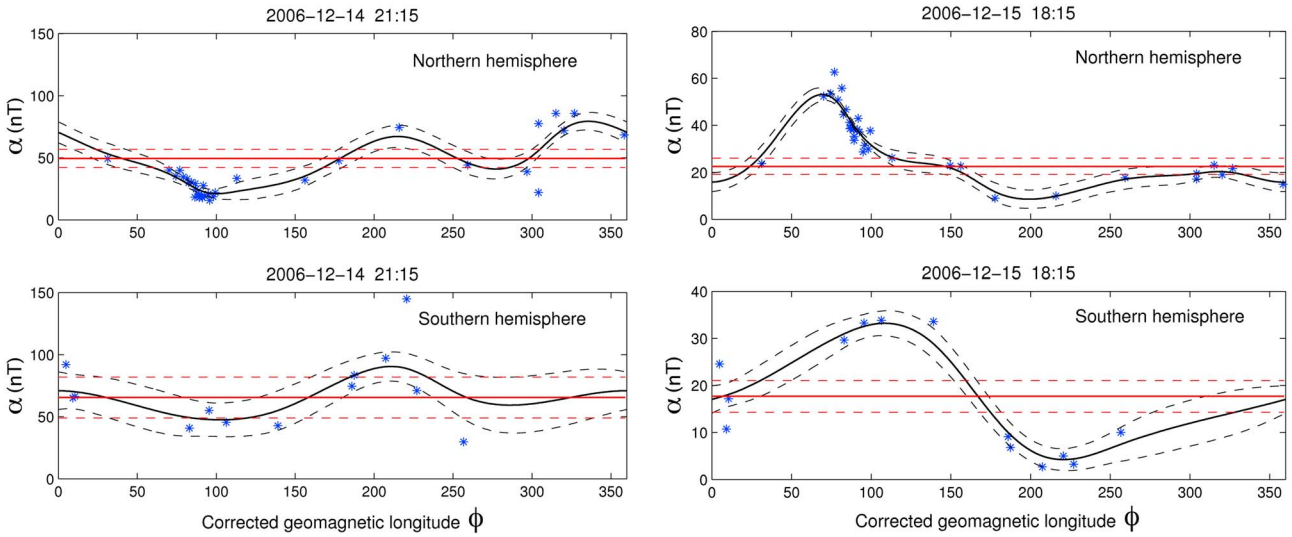

Figure 6. Variations over CGM longitude ϕ of the magnetic activity of all subauroral stations used in the α_{15} network, after rescaling at 50° CGM latitude through the correction factor cor. Two different intervals are displayed for the (top row) Northern and (bottom row) Southern Hemispheres: (left column) 14 December 2006 and (right column) 15 December 2006. The black curves correspond to cubic B-spline fittings associated with all the stations, and the two dashed curves correspond to the pointwise confidence interval also derived using the B-spline expression. The horizontal red lines represent the mean magnetic activity over the whole hemisphere, and the two dashed lines are the mean confidence interval.

Figure 6 presents examples of this spline fitting procedure for two 15 min intervals in December 2006 and for both hemispheres. On each panel of this figure, the blue crosses correspond to the corrected ΔH_{15} values of each station, the continuous black curve corresponds to the smoothed cubic spline $\alpha_{15}(\phi)$ function, and the dashed curves correspond to the upper and lower limits of the estimated confidence interval. For both intervals, one can observe that the $\alpha_{15}(\phi)$ functions have similar shapes in the Northern and Southern Hemispheres, with minimum values around 100° CGM longitude on 14 December 21:15 UT and 200° CGM longitude on 15 December 18:15 UT, despite the fairly large confidence interval obtained in the Southern Hemisphere on 14 December 2006 (Figure 6, bottom left).

3.3. Hemispheric α_{15} Index Calculation

For each 15 min interval, the hemispheric α_{15N} and α_{15S} indices are obtained by averaging over the longitude. A planetary index α_{15} is also obtained as the mean value of the two hemispheric indices (i.e., $\left(\alpha_{15N} + \alpha_{15S}\right)/2$).

The $\alpha_{15}(\phi)$ functions represent accurately the variation of the magnetic activity along with longitude at subauroral latitudes. One may argue that, in this case, the use of cubic spline appears complicated, while a simple mean would nearly give the same hemispheric value. This last point is not entirely accurate, because the observatories are not evenly distributed in longitude and because this distribution will change from one year to the other. The use of spline prior to calculation of a hemispheric mean allows to mitigate the influence of stations distribution along with longitude and not to overestimate, in the computation of the planetary α_{15} index, the geomagnetic activity in regions where the density of observatories is large (as in Europe) compared to that in regions where this density is low (e.g., Pacific Ocean). The use of cubic spline allows to switch from a discrete, unevenly distributed space up to a continuous regular one.

In the following sections, we chose to remain focused on the statistical study of hemispheric and planetary indices and to compare them with the *am* ones. We have used the indices over the 2000–2009 period where the new α_{15} indices are computed with a sufficient number of observatories in both hemispheres.

4. Statistical Characterization of α_{15} Indices

4.1. Characterization of α_{15} Indices Over a Solar Cycle

In this subsection, we present the statistical distribution of magnetic activity values recorded by the α_{15} indices by using probability distribution function (PDF). Figure 7 (first panel) presents the PDF of northern and southern hemispheric α_{15N} and α_{15S} indices over the 2000–2009 period. Bins of 0.25 nT are used up to 20 nT; above this value, the number of samples drops significantly and all higher activity values have been gathered in a unique bin. These PDF values show a strongly asymmetric distribution with a maximum position around

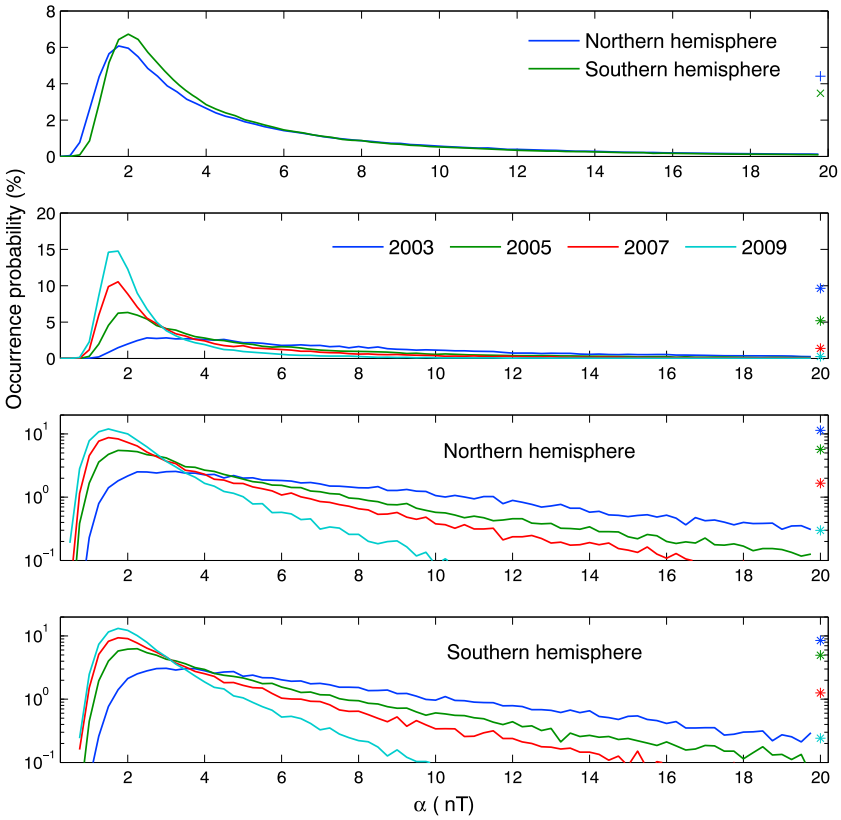

Figure 7. Probability distribution functions (PDF) of (first panel) the values of northern (blue) and southern (green) hemispheric α_{15} indices over the entire period 2000 to 2009; the values (second panel) of planetary α_{15} indices, (third panel) of α_{15N} indices, and (fourth panel) of α_{15S} indices for four different years: 2003 (blue), 2005 (green), 2007 (red), and 2009 (cyan). Bins of 0.25 nT on the horizontal axis are used. A linear scale on the vertical axis is used in the first and second panels, while a logarithmic scale is used in the third and fourth panels.

2 nT value and a long tail extending toward high-activity values. In the very low activity range (α_{15} smaller than or equal to 1.5 nT), PDF values are smaller in the Southern Hemisphere than in the Northern Hemisphere. PDF values then become larger in the Southern Hemisphere around the maximum of the distribution; this maximum is wider and occurs at a slightly higher value for α_{15S} than for α_{15N}. In the high-activity range, PDF values are again smaller in the Southern Hemisphere than in the Northern Hemisphere: this is clearly illustrated by the bin of α_{15} values larger than 20 nT (shown by the two symbols close to the right vertical axis). For this bin, the difference of about 1% in the number of points above 20 nT between Northern and Southern Hemispheres is meaningful, as it represents about 3500 samples. The reason for this statistically higher activity in the Northern Hemisphere than in the Southern Hemisphere is difficult to interpret as it could have a physical origin, magnetic activity being globally lower in the Southern than in the Northern Hemisphere [*Mayaud*, 1980; *Menvielle*, 1979], and/or it could be a network effect where the lower number of stations in the Southern Hemisphere would give a poorer description of subauroral activity.

To check the influence of the network, we have made a first series of tests. For a few case studies, we have removed stations in the Northern Hemisphere, to get as many stations as in the Southern Hemisphere, then we have recalculated the cubic spline fitting in the Northern Hemisphere. The new α_{15N} obtained with this poorer network of stations still remains higher in intensity than α_{15S}, giving more credit to the physical origin of this discrepancy. However, such results will be more carefully investigated in a future study.

In Figure 7, we show also the PDF of the α_{15} indices for 4 years encompassing the variations observed during the last solar cycle. The second panel presents a comparison of the PDF of planetary α_{15} using a linear scale. Although the PDF shape remains globally similar for the different years, the 2003 PDF is very broad with few values in the low-activity range, while on the contrary the 2009 PDF is highly peaked around 1.5 nT. The 2005 and 2007 PDF display an intermediate shape. Let us note that the peak value decreases with increasing solar

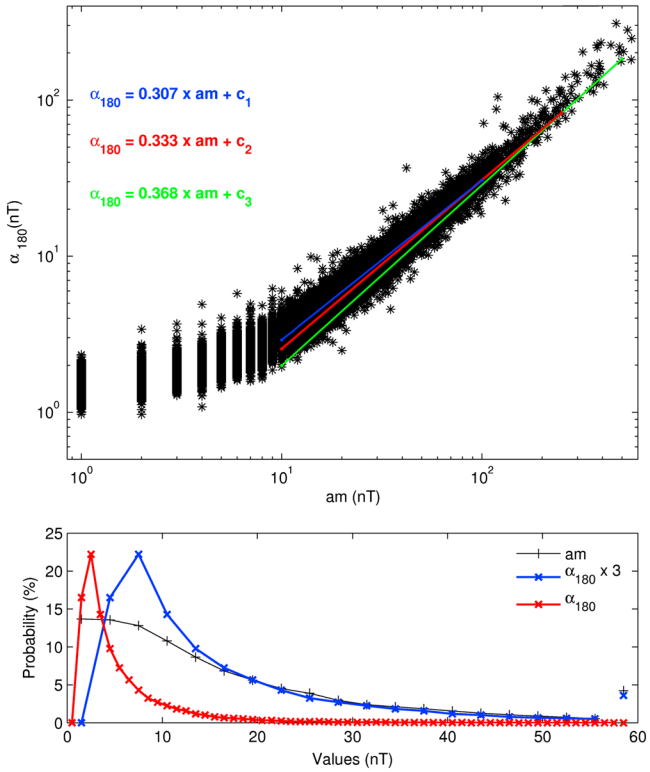

Figure 8. (top) Scatter diagram of *am* and corresponding α_{180} values for the entire period 2000 to 2009. The colored line corresponds to the linear relationships calculated for *am* values between 10 and 100 nT (blue), 10 and 250 nT (red), and 10 and 500 nT (green) and resulting in a mean scaling factor of 3 between the two sets of indices. (bottom) Probability distribution functions (PDF) of the values of *am* (black) and planetary α_{180} (blue) indices multiplied by 3 and planetary α_{180} (red) indices, for the entire period 2000 to 2009.

activity, while the bin where this maximum is observed is shifted toward higher α_{15} values. The PDF of α_{15S} and α_{15N} are compared in the third and fourth panels; a logarithmic scale is used to outline the high similitude between them. For each year, PDF maximum values are lower in the Northern Hemisphere than in the Southern Hemisphere, as observed previously for the entire solar cycle. Moreover, the relative variations of PDF shapes from one year to another are similar in the two hemispheres. This is also true for high geomagnetic activity level, as shown by the stars which count the number of α_{15} values above 20 nT. This fact proves that the relative variations of the α_{15} index calculation in the Southern Hemisphere is reliable, despite the small number of observatories.

4.2. Statistical Comparison Between Planetary α_{180} and *am* Indices

The planetary α_{15} index has been averaged over 3 h (α_{180}) in order to have a first quantitative comparison with *am* index. Figure 8 (top) shows the scatter diagram of *am* and α_{180} for the period 2000 to 2009. Linear relationships (shown by the colored lines) have been calculated for *am* values between 10 and 100 nT (blue curve), between 10 and 250 nT (red curve), and between 10 and 500 nT (green curve); i.e., for, respectively, 58.9%, 59.8%, and 59.9% of the 29,208 data points. A mean scaling factor of about 3 is thus found between the two kinds of indices.

This factor is due to the averaging procedure used for α_{15} calculation as compared to the use of a maximum range value during a 3 h interval for *am* calculation.

Figure 8 (bottom) shows again the PDF of the values of *am* and planetary α_{180} indices for the years 2000 to 2009. For α_{180}, we show the PDF estimated directly with this new index (red curve), but also the PDF estimated using the scaling factor of 3 (α_{180} is multiplied by 3) (blue curve) and accordingly for the bin width: 1nT for α_{180} and 3 nT for [$\alpha_{180} \times 3$] and for *am* indices. The α_{180} PDF has a peak value at very low magnetic activity around 3–4 nT and drops very quickly to low probability value above about 15 nT, making comparison with the *am* PDF complicated. On the other hand, after multiplying α_{180} by 3, the comparison becomes easier and shows

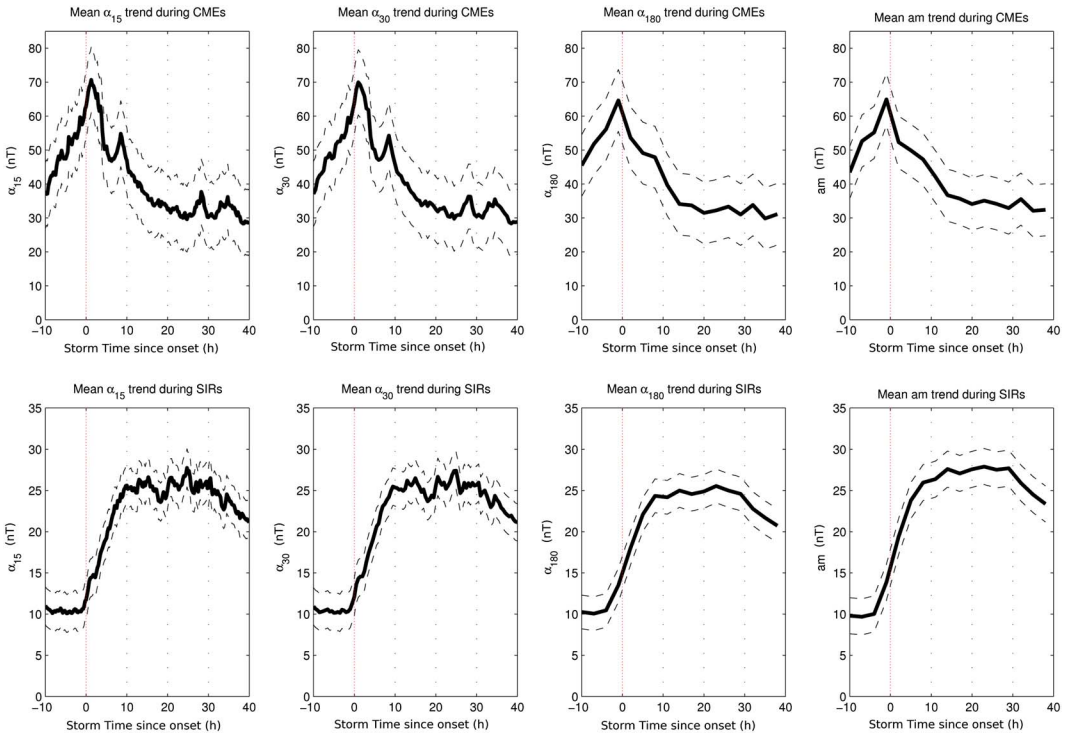

Figure 9. Superposed epoch analysis (SEA) for (top row) interplanetary coronal mass ejections (ICMEs) and (bottom row) stream interaction regions (SIR), over 2000–2009. The two dashed curves represent the 2 sigma confidence interval. (left to right) The results for α_{15}, α_{30}, α_{180} and *am* (α indices being multiplied by 3).

that the $[\alpha_{180} \times 3]$ and *am* PDF are not statistically different for $am > 15$ nT (i.e., $\alpha_{180} > 5$ nT). The two symbols close to the right axis of the plot count all the values larger than 60 nT for *am* and $[\alpha_{180} \times 3]$. This number of samples is of the same order for both indices and corresponds to slightly less than 5% of the points. These PDF values show that *am* and α_{180} describe similarly moderate and high levels of magnetic activity. On the contrary, the $[\alpha_{180} \times 3]$ and *am* PDF are different for $am < 15$ nT (i.e., $\alpha_{180} < 5$ nT): the $[\alpha_{180} \times 3]$ PDF is more peaked than the *am* one, with a peak value about 2 times larger for $[\alpha_{180} \times 3]$ (~22%) than for *am* (~13%). In fact, fewer intervals with low activity are recorded for *am* than for α_{180}. But this shift toward low values of α_{180} disappear for $[\alpha_{180} \times 3]$ simply because of the multiplying factor of 3. The explanation for these differences at low magnetic activity lies in the different algorithms of these two indices. During a quiet 3 h interval, a very localized activity peak will result in a higher *am* value, since the *am* calculation is based on the sum of the maximum positive and negative deviations (range) during the 3 h period, while the average of the α_{15} values over the 3 h will smooth out this localized peak and will give a lower α_{180} value.

4.3. Statistical Behavior of α During Strong Magnetic Activity and Comparison With *am*

In order to study how the new α family of indices behave during strong magnetic activity such as storms, we have performed superposed epoch analysis (SEA) of α and *am* for all interplanetary coronal mass ejections (ICMEs) as defined by *Cane and Richardson* [2003] and *Richardson and Cane* [2010] and all stream interaction regions (SIR) as defined by *Jian et al.* [2006, 2011]. Both lists have been regularly updated on the web and contain, respectively, 228 ICMEs and 389 SIRs over 2000–2009. Figure 9 presents the results of these SEAs for ICMEs on the top row and SIRs on the bottom row, the two dashed curves representing the 2 sigma confidence interval. From left to right are displayed the results for α_{15}, α_{30} (corresponding to α_{15} averaged over 30 min), α_{180}, and *am*. Again, as for Figure 8 (bottom), α values have been multiplied by 3 to ease the comparison with *am*. All indices display fairly well the same global profile. For SIRs-driven storms, magnetic activity shows a relatively smooth ramp lasting for almost 10 h, followed by a 20 h plateau with intermediate magnetic values, before starting to decrease. This behavior is typical of SIRs, where sustained high-speed solar wind enhances its coupling efficiency with the Earth's magnetosphere. For ICMEs-driven storms, magnetic activity shows a stronger (twice more intense than the SIRs) and shorter response, as the activity drops quickly 15 h after the ICMEs onset time. On the other hand, magnetic activity increases almost 10 h before the onset time, but it is

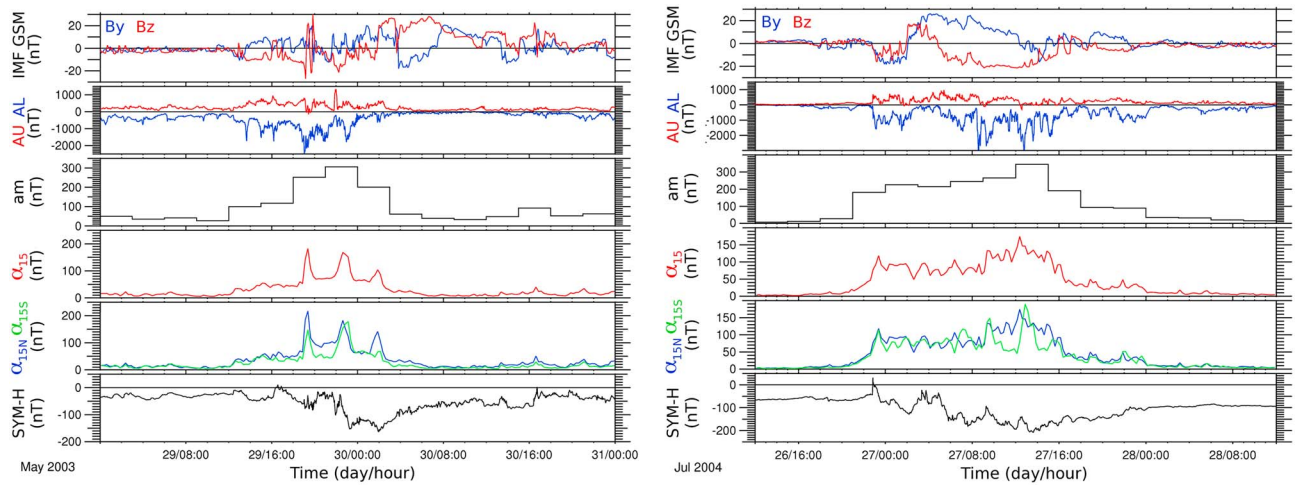

Figure 10. Solar wind parameters and geomagnetic indices during the (left column) 29 May 2003 and (right column) 27 July 2004 storms. (top to bottom) The *Y* and *Z* components of the IMF in geocentric solar magnetospheric (GSM) coordinates, the *AU* and *AL* indices, the *am* index, the planetary α_{15} index, the α_{15N} and α_{15S} hemispheric indices, and the *SYM-H* index.

well known that sheath activity ahead of ICMEs can strongly enhance magnetic activity even before the ICMEs arrival at the Earth.

By comparing SEAs, it is clear that increasing the time resolution of the α family of indices allows to better assess the onset and the development phase of the storms. Thus, for SIRs-driven storms, the magnetic activity onset aligns nicely with the onset time defined by *Jian et al.* [2006] (dotted vertical line on each plot) for α_{15} and α_{30}, while the magnetic activity ramp initiates well before the onset time for α_{180} and *am*. For ICMEs-driven storms, we can remark that the maximum of activity is found just after the ICMEs onset time for α_{15} and α_{30}, while it is found just before for α_{180} and *am*. The comparison between SEAs performed with α_{15} and α_{30} clearly shows that a 30 min resolution is sufficient to describe properly the magnetic activity during strong events, at least on a statistical basis. The comparison between SEAs performed over α_{180} and *am* are strikingly similar to within the scaling factor of 3. For ICMEs, the maximum value reached is about 64.5 nT for *am* and about 21.5 nT for α_{180} and for SIRs, the maximum value reached is about 28 nT for *am* and about 8.5 nT for α_{180}. Finally, the ICMEs and SIRs SEAs for hemispheric α_{15} (not shown) display the same behavior but with again stronger α_{15N} values than α_{15S}, as already observed with the PDF (see subsection 4.1).

5. Two Geomagnetic Storms Case Studies

In order to highlight the behavior of the new hemispheric and global α_{15} indices with respect to previous existing indices, we present two geomagnetic storms of the last solar cycle (29 May 2003 and 27 July 2004), each preceded and followed by periods of magnetic quietness. For each storm, Figure 10 (top to bottom) displays the IMFB_y and IMFB_z components, the *AU* and *AL* indices, the *am* index, the planetary α_{15} index, the hemispheric α_{15N} and α_{15S} indices, and the *SYM-H* index. These two storms have been already studied by *Hanuise et al.* [2006] for the first one and by *Kataoka and Miyoshi* [2008] for the second one, and in consequence, we will mainly focus on the new signatures provided by the α_{15} indices. For both events, the α_{15} indices clearly show far more details than the historical *am* index, in storm periods as well as in quiet periods. The α_{15N} index is always higher than the α_{15S} index, which can be explained partly by the fact that magnetic activity recorded by α_{15} is always higher in the Northern Hemisphere (see previous section) and partly by the season: both storms occur close to the summer solstice in the Northern Hemisphere, implying more solar illumination and thus strongest response in the north. The α_{15} indices aim to provide an integrated view of terrestrial magnetic activity; however, comparing with other indices allows to infer which current contribution will dominate over the others.

For the first storm (Figure 10, left column), three successive halo coronal mass ejections (CMEs) formed a large south-north magnetic cloud lasting more than 26 h which hit the Earth on 29 May 2003 around 12:00 UT. The counterpart geomagnetic storm lasted only about 18h until 06:00 UT (30 May) since the geoeffectivity is restricted to the southern part of the magnetic cloud. Intense solar wind pressure pulses (up to 75 nPa) and

interplanetary shocks (not shown) are also detected during the magnetic cloud. During the storm, *am* only displays a single peak at about 300 nT around 22:00 UT (29 May), while *AU* and *AL* show at least six negative peaks due to successive northern auroral intensifications. Finally, *SYM-H* displays a complex main phase decreasing to less than 160 nT, followed by a smooth recovery phase during the northern part of the magnetic cloud. The α_{15} indices display three main peaks up to almost 180 nT. The first and stronger peak at about 19:00 UT (29 May) and the next 3h of activity are more intense in the Northern than in the Southern Hemisphere and are clearly associated with the strongest *AL* index. The α_{15} indices most probably react here to the auroral electrojets intensification, the Northern Hemisphere having a strongest response due to the higher solar illumination during this season. The second peak shows equivalent response in amplitude in both hemispheres but with a delay of about 30 min observed in the Southern Hemisphere. This peak occurs during the strongest *SYM-H* gradient of the main phase, meaning that the α_{15} indices most probably react here to the ring current, which could explain the symmetrical signatures in amplitude observed in both hemispheric α_{15} indices. The 30 min delay observed between the hemispheric indices is clearly a very interesting and new feature which seems to be relatively common during magnetic storms. It will be extensively investigated in a further study. Finally, the third peak is still very intense in the Northern Hemisphere while almost nonexistent in the Southern Hemisphere. However, it occurs at the end of the main storm phase, when not much auroral activity is recorded by *AU* and *AL*. This third peak is probably a consequence of ring current intensification, but the strong asymmetry observed between hemispheric indices is more difficult to interpret and could be due either to a failing of the spline fitting in the Southern Hemisphere due to the poor number of stations or to a complex combination of different current signatures such as field-aligned currents which are known to have strong amplitude difference between hemispheres during solstice [*Green et al.*, 2009]. The α_{15} indices drop very quickly after the beginning of the recovery phase.

For the second storm (Figure 10, right column), a geoeffective sheath followed by a very fast magnetic cloud associated with a CME hits the Earth on 26 July 2004 around 23:00 UT. The magnetic cloud shows a slow north-south magnetic rotation. A high pressure (20 nPa) and fast speed are also observed in the solar wind (not shown). This storm also lasts about a day but shows a far more sustained activity due to the long negative IMFB_z periods (sheath and end of cloud). The *AL*, *am*, and *SYM-H* indices show complex variations: *AL* shows more than eight negative peaks, *am* maintains intense values (> 200 nT) for half a day, while *SYM-H* displays successive phases of decreasing and recovery phases during the same period. The α_{15} indices display the same sustained activity than *am*, reaching about 170 nT around 13:00 UT (27 July). Up to 08:00 UT (27 July), both hemispheric indices show almost the same behavior and probably record a combination of auroral electrojets and ring current intensifications. After the peak at 09:00 UT (27 July), α_{15S} drops with respect to α_{15N} and *AL* shows strong negative values. The α_{15} indices most probably react here to the auroral electrojets intensification, with again strongest response in the north due to the season. The peak at about 13:00 UT (27 July) shows almost the same amplitude in both hemispheres, implying that the ring current contribution could dominate here, but again a delay of about 30 min is observed for α_{15S} over α_{15N}. Again, the α_{15} indices drop very quickly after the beginning of the recovery phase, although small α_{15} and *AL* intensifications are observed when IMFB_z turns negative.

A more detailed study of the behavior of the α_{15} indices is outside the scope of this paper, but through these two storm examples, we have shown the ability of these indices to describe more precisely the complex regional electrodynamics of the magnetosphere-ionosphere system driven by solar wind interaction.

6. Conclusion

The new α_{15} indices rely on a simple and flexible calculation algorithm. We took advantage of the experience gained in the calculation of IAGA-endorsed geomagnetic indices at subauroral latitudes and intend to mitigate their historical drawbacks. Indeed, the new α_{15} indices (i) are not based on an unchangeable network but at contrary remain valid even if the stations network is modified over time; (ii) are taking into account the main field secular variation introduced by the change with time of the magnetic stations CGM coordinates; (iii) are derived every 15 min which allows a good temporal resolution of magnetic perturbations description (storms and substorms) while being not sensitive to magnetic pulsations; and (iv) are calculated for each hemisphere separately with a straightforward determination of planetary indices.

The PDF statistical results underline clearly a similar magnetic activity distribution on planetary and hemispheric scales. Moreover, as expected, the magnetic activity distribution of the indices is clearly shifted

toward higher activity during the maximum of the solar cycle. From SEAs results, it appears that increasing the temporal resolution of the subauroral indices, from 3 h up to 15 min, allows to finely describe the different phases of storm events. The comparison of the new α_{15} index averaged over 3 h with the historical *am* index is very satisfactory on a statistical basis for all levels of magnetic activity. Case studies of two specific geomagnetic events show that comparisons in regard to other parameters, such as other magnetic indices and IMF parameters, confirm that the new α_{15} indices correctly restore and enhance subauroral magnetic activity description.

From now on, the planetary and hemispheric α_{15} index series are preliminary and available for the 1996–2009 period. However, due to the smallest number of stations and to the poor access to digital data before 1996, it will not be possible to go back earlier in time (at least for the Southern Hemisphere), and in consequence, the α_{15} index will not be usable yet to study secular variations of terrestrial magnetic activity. In the very near future, we will extend the calculation to current days and will settle an automated computation to obtain preliminary and quicklook α_{15} values, just a few minutes after the end of the current interval. Indeed, the clear and simple algorithm is critical for real-time index calculation for space weather purposes.

The development of the new α_{15} indices is a further step toward new geomagnetic indices with better temporal and spatial resolution. Additional research should be undertaken to validate irrevocably the gainings brought by the α_{15} indices through, for example, more case studies for different levels of magnetic activity. Moreover, taking advantage of the performance of the cubic splines adjustment, further studies are already planned to investigate in detail the longitudinal variations of subauroral magnetic activity.

This new type of indices is a possible answer to the recent needs of the community to better characterize magnetic activity in models (internal magnetic field, radiation belts, ionosphere...) as well as for magnetic storms study. We hope that the new α_{15} indices will be useful and widely used by the scientific community. These indices are available and may be downloaded at the following web address: http://cdg.u-strasbg.fr/PortailEOST/Mag/ObsMag-data.html.

Acknowledgments

This work was supported by the CNES. The results presented in this paper rely on data collected at magnetic observatories. We thank the national institutes that support them and INTERMAGNET for promoting high standards of magnetic observatory practice (www.intermagnet.org). The results presented in this paper rely on *am* geomagnetic index calculated by LATMOS, Guyancourt, France, and recently EOST, Strasbourg, France, from data collected at magnetic observatories, and made available through International Service of Geomagnetic Indices (ISGI) Web site: http://isgi.unistra.fr. Data analysis presented in Figure 10 was performed with the AMDA science analysis system provided by the Centre de Données de la Physique des Plasmas (CDPP) supported by CNRS, CNES, Observatoire de Paris and Université Paul Sabatier, Toulouse. We would like to thank the two anonymous reviewers for their suggestions and comments.

References

Bartels, J., N. H. Heck, and H. F. Johnston (1939), The three-hour-range index measuring geomagnetic activity, *J. Geophys. Res.*, *44*, 411–454, doi:10.1029/TE044i004p00411.

Bartels, J. (1949), *The Standardized Index, Ks, and the Planetary Index, Kp, IATME Bull., 12b*, 97 pp., Int. Union of Geod. and Geophys. (IUGG), Paris.

Cane, H. V., and I. G. Richardson (2003), Interplanetary coronal mass ejections in the near Earth solar wind during 1996–2002, *J. Geophys. Res.*, *108*(A4), 1156, doi:10.1029/2002JA009817.

Chambodut, A., A. Marchaudon, M. Menvielle, F. El-Lemdani Mazouz, and C. Lathuillère (2013), The *K*-derived MLT sector geomagnetic indices, *Geophys. Res. Lett.*, *40*, 4808–4812, doi:10.1002/grl.50947.

Cliver, E. W., Y. Kamide, and A. G. Ling (2000), Mountains versus valleys: Semiannual variation of geomagnetic activity, *J. Geophys. Res.*, *105*(A2), 2413–2424.

Constable, S., and C. Constable (2004), Observing geomagnetic induction in magnetic satellite measurements and associated implications for mantle conductivity, *Geochem. Geophys. Geosyst.*, *5*, Q01006, doi:10.1029/2003GC000634.

Davis, T. N., and M. Sugiura (1966), Auroral electroject activity index *AE* and its universal time variations, *J. Geophys. Res.*, *71*, 785–801, doi:10.1029/JZ071i003p00785.

Friis-Christensen, E., H. Lühr, and G. Hulot (2006), Swarm: A constellation to study the Earth's magnetic field, *Earth Planets Space*, *58*(4), 351–358.

Gannon, J. L., and J. J. Love (2011), USGS 1-min *Dst* index, *J. Atmos. Sol. Terr. Phys.*, *73*, 323–334.

Gjerloev, J. W. (2012), The SuperMAG data processing technique, *J. Geophys. Res.*, *117*, A09213, doi:10.1029/2012JA017683.

Green, D. L., C. L. Waters, B. J. Anderson, and H. Korth (2009), Seasonal and interplanetary magnetic field dependence of the field-aligned currents for both Northern and Southern Hemispheres, *Ann. Geophys.*, *27*, 1701–1715, doi:10.5194/angeo-27-1701-2009.

Haaland, S., and J. Gjerloev (2013), On the relation between asymmetries in the ring current and magnetopause current, *J. Geophys. Res. Space Physics*, *118*, 7593–7604, doi:10.1002/2013JA019345.

Hakura, Y. (1965), Tables and maps of geomagnetic coordinates corrected by the higher order spherical harmonic terms, Rept. Ionosphere Space Res. Jpn., vol. 19, Radio Res. Lab., Kokubunji, Tokyo.

Hanuise, C., et al. (2006), From the Sun to the Earth: Impact of the 27–28 May 2003 solar events on the magnetosphere, ionosphere and thermosphere, *Ann. Geophys.*, *24*, 129–151.

Iyemori, T. (1990), Storm-time magnetospheric currents inferred from mid-latitude geomagnetic field variations, *J. Geomag. Geoelectr.*, *42*, 1249–1265.

Jian, L., C. T. Russell, J. G. Luhmann, and R. M. Skoug (2006), Properties of stream interactions at one AU during 1995–2004, *Sol. Phys.*, *239*(1–2), 337–392, doi:10.1007/s11207-006-0132-3.

Jian, L. K., C. T Russell, and J. G. Luhmann (2011), Comparing solar minimum 23/24 with historical solar wind records at 1 AU, *Sol. Phys.*, *274*(1–2), 321–344, doi:10.1007/s11207-011-9737-2.

Kataoka, R., and Y. Miyoshi (2008), Average profiles of the solar wind and outer radiation belt during the extreme flux enhancement of relativistic electrons at geosynchronous orbit, *Ann. Geophys.*, *26*, 1335–1339.

Katus, R. M., and M. W. Liemohn (2013), Similarities and differences in low-to-middle latitude geomagnetic indices, *J. Geophys. Res. Space Physics*, *118*, 5149–5156, doi:10.1002/jgra.50501.

Kerridge, D. J. (2001), INTERMAGNET: Worldwide Near-Real-Time Geomagnetic Observatory Data. Proc. ESA Space Weather Workshop, ESTEC, Noordwijk, Netherlands. [Available at http://www.intermagnet.org/publications/IM_ESTEC.pdf.]

La Sayette, P., and A. Berthelier (1996), The *am* annual-diurnal variations 1959–1988: A 30-year evaluation, *J. Geophys. Res.*, *101*(A5), 10,653–10,663.

Laundal, K. M., and J. W. Gjerloev (2014), What is the appropriate coordinate system for magnetometer data when analyzing ionospheric currents?, *J. Geophys. Res. Space Physics*, *119*, 8637–8647, doi:10.1002/2014JA020484.

Lockwood, M. (2013), Reconstruction and prediction of variations in the open solar magnetic flux and interplanetary conditions, *Living Rev. Sol. Phys.*, *10*, 4, doi:10.12942/lrsp-2013-4.

Mayaud, P.-N. (1968), *Indices Kn, Ks et Km, 1964–1967*, 156 pp., C.N.R.S., Paris.

Mayaud, P.-N. (1973), *A Hundred Year Series of Geomagnetic Data, 1868–1967: Indices AA, Storm Sudden Commencements*, 33 pp., IAGA Bull., IUGG, Paris.

Mayaud, P.-N. (1980), *Derivation, Meaning and Use of Geomagnetic Indices, Monograph 22*, AGU, Univ. of Calif.

Menvielle, M. (1979), A possible geophysical meaning of *K* indices, *Ann. Geeophys.*, *35*, 189–196.

Menvielle, M., and J. Paris (2001), The aλ longitude sector geomagnetic indices, *Contrib. Geophys. Geod.*, *31*, 315–322.

Menvielle, M., N. Papistashvili, L. Hakkinen, and C. Suckdorff (1995), Computer production of *K* indices: Review and comparison of methods, *Geophys. J. Int.*, *123*(3), 866–886, doi:10.1111/j.1365-246X.1995.tb06895.x.

Menvielle, M., T. Iyemori, A. Marchaudon, and M. Nose (2011), Geomagnetic observations and models, in *Geomagnetic Observations and Models, IAGA Special Sopron Book Series*, vol. 5, edited by M. Mandea and M. Korte, Springer, Netherlands, doi:10.1007/978-90-481-9858-0_8.

Newell, P. T., and J. W. Gjerloev (2011a), Evaluation of SuperMAG auroral electrojet indices as indicators of substorms and auroral power, *J. Geophys. Res.*, *116*, A12211, doi:10.1029/2011JA016779.

Newell, P. T., and J. W. Gjerloev (2011b), Substorm and magnetosphere characteristic scales inferred from the SuperMAG auroral electrojet indices, *J. Geophys. Res.*, *116*, A12232, doi:10.1029/2011JA016936.

Newell, P. T., and J. W. Gjerloev (2012), SuperMAG-based partial ring current indices, *J. Geophys. Res.*, *117*, A05215, doi:10.1029/2012JA017586.

Nosé, M., et al. (2012), Wp index: A new substorm index derived from high-resolution geomagnetic field data at low latitude, *Space Weather*, *10*, S08002, doi:10.1029/2012SW000785.

Richardson, I. G., and H. V. Cane (2010), Near-Earth interplanetary coronal mass ejections during solar cycle 23 (1996–2009): Catalog and summary of properties, *Sol. Phys.*, *264*(1), 189–237, doi:10.1007/s11207-010-9568-6.

Silverman, B. W. (1985), Some aspects of the spline smoothing approach to non-parametric regression curve fitting, *J. R. Stat. Soc.*, *47*(1), 1–52.

Singh, A. K., R. Rawat, and B. M. Pathan (2013), On the UT and seasonal variations of the standard and SuperMAG auroral electrojet indices, *J. Geophys. Res. Space Physics*, *118*, 5059–5067, doi:10.1002/jgra.50488.

Sucksdorff, C., R. Pirjola, and L. Häkkinen (1991), Computer production of *K*-values based on linear elimination, *Geophys. Trans.*, *36*, 333–345.

Sugiura, M. (1965), Hourly values of equatorial *Dst* for the IGY, *Ann. Int. Geophys. Year*, *35*, 9–45.

Svalgaard, L. (1977), Geomagnetic activity: Dependence on solar wind parameters, in *Skylab Workshop Monograph on Coronal Holes*, edited by J. B. Zirker, chap. 9, 371 pp., Columbia Univ. Press, New York.

Thébault, E., et al. (2015), International geomagnetic reference field: The twelfth generation, *Earth Planets Space*, *67*, 79, doi:10.1186/s40623-015-0228-9.

Thomson, A. W. P., and V. Lesur (2007), An improved geomagnetic data selection algorithm for global geomagnetic field modelling, *Geophys. J. Int.*, *169*, 951–963, doi:10.1111/j.1365-246X.2007.03354.x.

Troshichev, O. A., V. G. Andrezen, S. Vennerstrom, and E. Friis-Christensen (1988), Magnetic activity in the polar cap—A new index, *Planet. Space Sci.*, *36*, 1095–1102, doi:10.1016/0032-0633(88)90063-3.